Cerebral Cortex, January 2017;27: 131–145

doi: 10.1093/cercor/bhw370
Advance Access Publication Date: 1 December 2016
Original Article

ORIGINAL ARTICLE

Synaptic Phospholipid Signaling Modulates Axon Outgrowth via Glutamate-dependent Ca^{2+}-mediated Molecular Pathways

Johannes Vogt[1], Sergei Kirischuk[2], Petr Unichenko[2], Leslie Schlüter[1], Assunta Pelosi[1], Heiko Endle[1], Jenq-Wei Yang[2], Nikolai Schmarowski[1], Jin Cheng[1], Carine Thalman[1], Ulf Strauss[3], Alexey Prokudin[1], B. Suman Bharati[1], Junken Aoki[4], Jerold Chun[5], Beat Lutz[6], Heiko J. Luhmann[2] and Robert Nitsch[1]

[1]Institute for Microscopic Anatomy and Neurobiology, University Medical Center, Johannes Gutenberg-University, 55131 Mainz, Germany, [2]Institute of Physiology, University Medical Center, Johannes Gutenberg-University, 55128 Mainz, Germany, [3]Institute of Cell Biology and Neurobiology, Charité – Universitätsmedizin, 10119 Berlin, Germany, [4]Graduate School of Pharmaceutical Sciences, Tohoku University, Sendai, Miyagi, 980-8578, Japan, [5]Dorris Neuroscience Center, The Scripps Research Institute, La Jolla, CA 92037, USA and [6]Institute of Physiological Chemistry, University Medical Center, Johannes Gutenberg-University, 55128 Mainz, Germany

Address correspondence to Robert Nitsch/Johannes Vogt, Institut für Mikroskopische Anatomie und Neurobiologie, Universitätsmedizin der Johannes Gutenberg-Universität Mainz, Langenbeckstr. 1, 55131 Mainz, Germany. Email: robert.nitsch@unimedizin-mainz.de (R.N.); johannes.vogt@unimedizin-mainz.de (J.V.)

J. Vogt, S. Kirischuk, and P. Unichenko contributed equally to this work.

Abstract

Altered synaptic bioactive lipid signaling has been recently shown to augment neuronal excitation in the hippocampus of adult animals by activation of presynaptic LPA_2-receptors leading to increased presynaptic glutamate release. Here, we show that this results in higher postsynaptic Ca^{2+} levels and in premature onset of spontaneous neuronal activity in the developing entorhinal cortex. Interestingly, increased synchronized neuronal activity led to reduced axon growth velocity of entorhinal neurons which project via the perforant path to the hippocampus. This was due to Ca^{2+}-dependent molecular signaling to the axon affecting stabilization of the actin cytoskeleton. The spontaneous activity affected the entire entorhinal cortical network and thus led to reduced overall axon fiber numbers in the mature perforant path that is known to be important for specific memory functions. Our data show that precise regulation of early cortical activity by bioactive lipids is of critical importance for proper circuit formation.

Key words: axon outgrowth, bioactive phospholipids, Ca2+-signaling, early synchronized activity, entorhinal–hippocampal formation

© The Author 2016. Published by Oxford University Press.
This is an Open Access article distributed under the terms of the Creative Commons Attribution Non-Commercial License (http://creativecommons.org/licenses/by-nc/4.0/), which permits non-commercial re-use, distribution, and reproduction in any medium, provided the original work is properly cited. For commercial re-use, please contact journals.permissions@oup.com

Introduction

The entorhinal–hippocampal projection (Amaral and Witter 1989) has gained special attention due to its importance for memory formation and spatial navigation (Moser et al. 2008). Formation of this pathway follows a precise spatiotemporal pattern of axon outgrowth (Del Rio et al. 1997). In the developing entorhinal cortex (EC), periodic spontaneous glutamate receptor-mediated events parallel the outgrowth of the entorhinal–hippocampal projection and show a characteristic time-locked increase during the first postnatal days (Sheroziya et al. 2009; Unichenko et al. 2015). In the early postnatal animal, space-encoding neurons show characteristic activity when the animal first starts to explore its environment, suggesting that the EC forms functional local excitatory connections to the hippocampus already during the early postnatal period (Langston et al. 2010). A role for early excitatory local activity in axon growth has been described in subcortical structures (Mire et al. 2012), indicating that early neuronal activity in the EC may be essential for the development of proper adult connectivity.

Glutamate not only acts as a neurotransmitter at excitatory synapses in the entorhinal–hippocampal system but also regulates axon growth (Yamada et al. 2008). Application of glutamate to the somatodendritic area induced axon retraction via calcium waves that propagated from the cell body to the growth cone (Yamada et al. 2008). This is in line with recent data showing that electrical activity induced by optogenetic stimulation decreased horizontal axon growth of cortical neurons (Malyshevskaya et al. 2013). Here, we show that glutamatergic signaling in the EC depending on proper regulation by synaptic bioactive phospholipid signaling critically influences axonal outgrowth and circuit formation via Ca^{2+}-dependent pathways. This signaling pathway is regulated by the postsynaptic molecule plasticity related gene 1 (PRG-1/PLPR4), which is an integral membrane protein and has a homology to lipid phosphate phosphatases, and is mediated via the presynaptic LPA_2-receptor (R) influencing glutamate release (Trimbuch et al. 2009). PRG-1 expression starts around birth (Brauer et al. 2003), concomitant with the development of the entorhinal–hippocampal perforant path (Del Rio et al. 1997), and increases towards the end of the second postnatal week (see Fig. S1a–c). This expression pattern suggests that entorhinal–hippocampal projection would be affected by increased glutamatergic transmission caused by PRG-1 deficiency. Indeed, in PRG-$1^{-/-}$ mice, which lack the postsynaptic PRG-1-dependent regulation of phospholipid signaling, we detected a premature appearance of early spontaneous glutamatergic activity in the EC by 2 days. This was mediated by presynaptic LPA_2-Rs and led to Ca^{2+}-dependent molecular signaling to the axon growth cone resulting in reduced axon growth velocity of entorhinal fibers. Reduced axon growth speed was due to specific alterations in Ca^{2+}-dependent signal transduction (Wayman et al. 2008) including increased phosphorylation of CaMKI but not of other members of the Ca^{2+}/Calmodulin(CaM)-pathway. A target of the Ca^{2+}/CaM-dependent protein kinases (Takemura et al. 2009; Saito et al. 2013), LimK1, which inactivates cofilin activity via phosphorylation (Mizuno 2013), showed reduced phosphorylation levels in the EC. Since cofilin negatively regulates actin dynamics and destabilizes axons via actin depolymerization (Mizuno 2013; Saito et al. 2013), reduced cofilin phosphorylation levels explain the negative effect on axon outgrowth of entorhinal fibers to the hippocampus. Our findings show that precise regulation of local excitatory networks is critical for circuit formation in the entorhinal–hippocampal connection mediated via Ca^{2+}-dependent axonal signaling pathways.

Materials and Methods

Transgenic Animals and Breeding

PRG-$1^{-/-}$ and PRG-$1^{-/-}$/LPA_2-$R^{-/-}$ mice and their littermate controls were obtained as described (Trimbuch et al. 2009). For coculture experiments, Thy-1.2-EGFP_L17 (Caroni 1997) and C57BL/6 TgN (ßact-EGFP) Osb 1 (Okabe et al. 1997) mice were crossbred with PRG-$1^{-/-}$ mice. All experiments involving animals were conducted in accordance with national laws for the use of animals in research and approved by the local ethical committee.

Ca^{2+}-Imaging and Electrophysiology In Vitro at P5

Slice preparation, extracellular field potential recordings, Ca^{2+}-imaging and single cell electrophysiology were performed according to standard procedures (Unichenko et al. 2015, 2016). EEPSCs were elicited by focal electrical stimulation through a glass pipette filled with the ACSF (~10 MΩ). The stimulation pipette was always positioned within layer 2 of MEC. N-(2,6-dimethylphenylcarbamoylmethyl)-triethylammonium bromide (QX 314, 2 mM) was added to the intracellular solution to prevent generation of action potentials in the tested neurons. An isolated stimulation unit was used to generate rectangular electrical pulses. Pulse duration was set to 0.2 ms. Pulse intensity was adjusted to activate a unitary synaptic input (minimal stimulation). Stimulation was accepted as minimal if the following criteria were satisfied: 1) eEPSC latency remained stable (<20% fluctuations), 2) lowering stimulus intensity by 20% resulted in a complete failure of eIPSCs, and 3) an increase in stimulus intensity by 20% changed neither mean eEPSC amplitude nor eEPSC shape. In addition, eEPSCs were inspected at a holding potential of −50 mV, Nernst Cl^- reversal potential. Depolarizing eEPSCs recorded at this membrane potential confirmed the glutamatergic nature of the evoked signals. Typical pulse intensity was between 2 and 4 μA.

Surgical Preparation and In Vivo Recordings in P5 Mice

Briefly, after 30–60 min recovery from the surgical procedure (Yang et al. 2013; Reyes-Puerta et al. 2015), a 4-shank 16-channel electrode (125 μm horizontal shank distance and 50 μm vertical inter-electrode distance, 1–2 MΩ; NeuroNexus Technologies) or an 8-shank 128-channel electrode (200 μm horizontal shank distance and 75 μm vertical inter-electrode distance, 1–2 MΩ; NeuroNexus Technologies) was inserted into cortical layer II/III of the anesthetized mouse to obtain FP recordings. One hour after the electrode was inserted into the EC, spontaneous activity was recorded for 1 h. Usually, spontaneous events were recorded from 1 to 2 groups of channels. The channel with maximum occurrence of spontaneous events was chosen for further analysis.

Data Analysis of In Vivo Recordings

FP data were imported and analyzed offline using MATLAB software version 7.7 (MathWorks). In each experiment, 900 s spontaneous extracellular local FP recording was used for the analysis. To detect spontaneous events, raw data were filtered between 1 and 80 Hz using a Butterworth 3-order filter. Spontaneous events were detected as FP deflections exceeding 5 times the baseline standard deviation (SD). The events were analyzed in their occurrence,

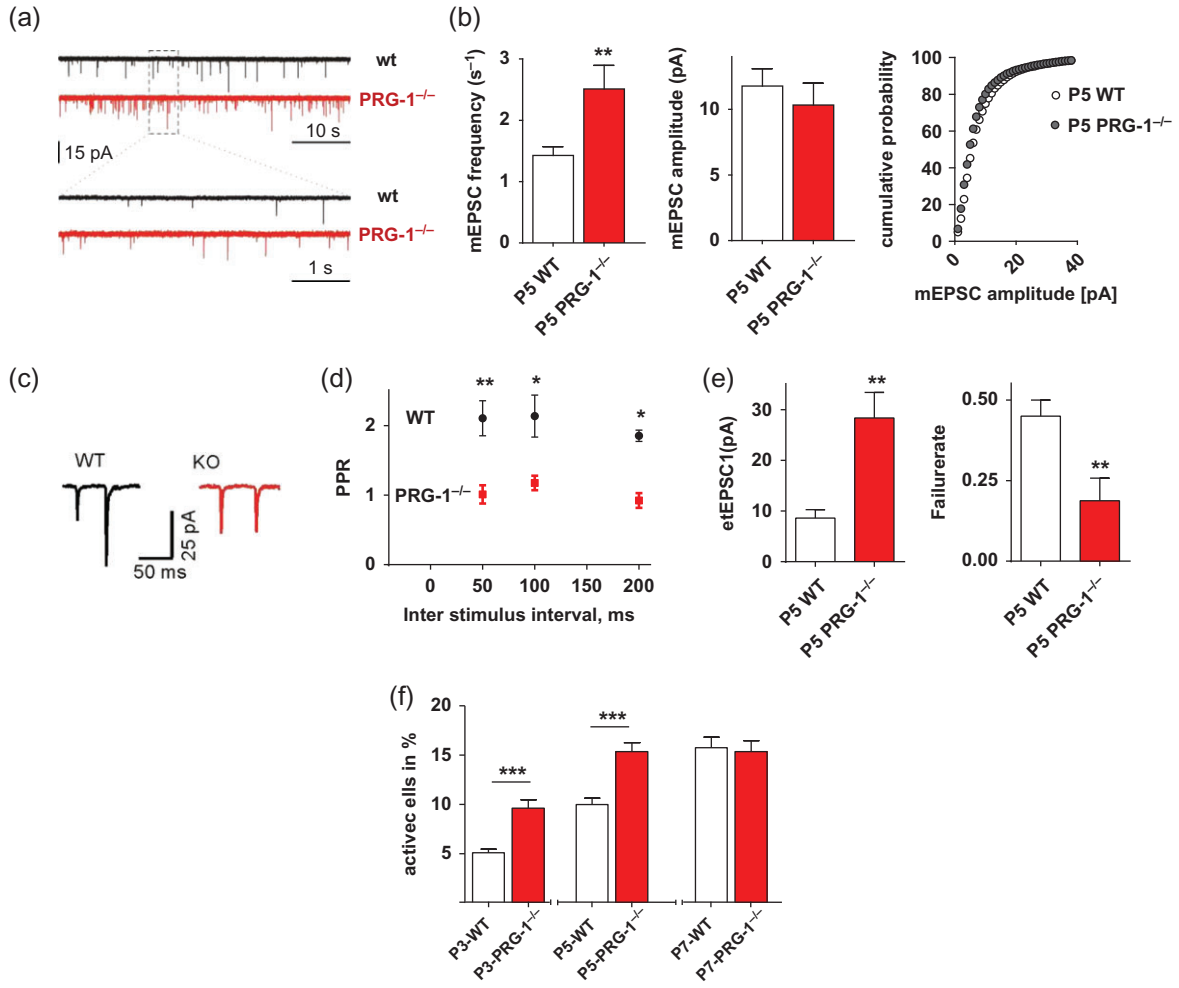

Figure 1. Altered phospholipid signaling regulating basal glutamatergic transmission increased neuronal firing probability in individual neurons. (*a*) Original traces showing mEPSCs from layer II/III pyramidal neurons voltage clamped at –70 mV. (*b*) Neurons from PRG-1$^{-/-}$ mice (n = 9 neurons) demonstrated more mEPSCs compared with those from their WT litters (n = 11 neurons), while average amplitude and cumulative mEPSC amplitude distribution of these events was similar between the 2 groups (Mann–Whitney test). (*c*) Representative averaged eEPSCs (20 trials in both cases) recorded from layer 2 MEC neurons in slices from P5 WT (black) and P5 PRG-1$^{-/-}$ (red) mice. (*d*) Dependence of the paired pulse ratio (PPR) on the interstimulus interval in slices from WT (black) and PRG-1$^{-/-}$ (red) animals. (*e*) Significantly larger eEPSC amplitudes (left panel) and smaller failure rates (right panel) were observed in slices from PRG-1$^{-/-}$ mice as compared with slices from WT littermates (n = 8 WT and 8 PRG-1$^{-/-}$ neurons, unpaired Student's t-test). (*f*) Quantitative analysis of active cell numbers identified by Ca^{2+}-imaging revealed significantly increased numbers of spontaneously active cells in layer II/III of the MEC in PRG-1$^{-/-}$ slices at P3 and P5 (P3, n = 27 WT and 30 PRG-1$^{-/-}$ slices, Mann–Whitney test; P5, n = 33 WT and 25 PRG-1$^{-/-}$ slices and P7, n = 23 WT and 27 PRG-1$^{-/-}$ slices, t-test). All data represent mean ± SEM. *P < 0.05, **P < 0.01; ***P < 0.001.

duration, and frequency with maximal fast Fourier transformation power within event. MUA was detected in 200 Hz highpass filtered signals by applying a threshold at 7 times the baseline SD. We calculate the MUA firing rate in channels located in MEC and further calculate the mean MUA firing rate from the channels with MUA firing rate >0.

Measurement of Axon Outgrowth Using Ex Vivo Organotypical Slice Cultures

Live-Imaging Measurements

Organotypic slice cultures containing EC from GFP-expressing transgenic mice and hippocampus from non-GFP transgenic mice were performed as described . After DIV3 cocultures were placed in a preheated chamber (37°C) aerated with humidified 5% CO_2 ambient air (Ludin chamber, Life Imaging Services). Imaging of outgrowing entorhinal axons in living slice cultures was performed using a microscope (TCS SP2, Leica) equipped with a 2-photon laser (Coherent, Titan: Saphire Chameleon). GFP fluorescence was obtained at an excitation wavelength of 900 nm and was imaged using a 20x water objective (Olympus XLUMPlanFL 0.95 NA). Axon growth velocity was calculated measuring the distance covered by single axons over time. Before imaging, slices were equilibrated for at least 1 h in the imaging chamber. Multiple optical sections (up to 30 sections, z-spacing of 0.8 µm) were collected every 10 min for up to 3 h. This observation condition did not induce photobleaching of GFP fluorescence nor did it alter axon outgrowth speed during the experiment. According to experimental conditions, 0.5 mM glutamate was directly applied to the medium. For data analysis, optical sections were reconstructed into single projection images for each time point using the maximum brightness operation of the Leica software. Each data point represents the outgrowth speed of 1 axon fiber. For analysis of the axon growth, individual axon growth speed during imaging was grouped in growth categories using the advance phase of WT→WT as a standard. According to axon outgrowth speed of WT axons at DIV3, the time axons grew with an axon growth

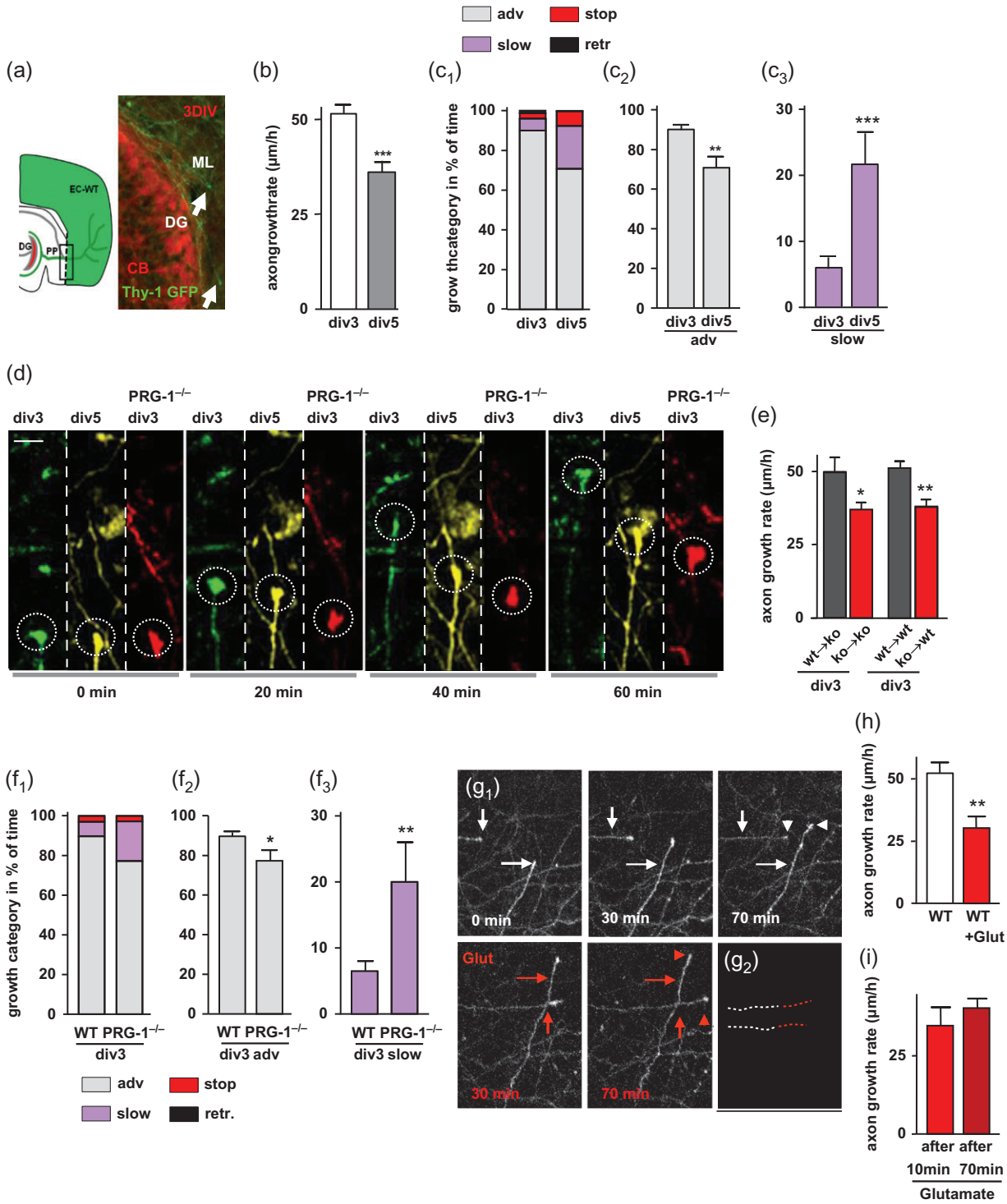

Figure 2. Increased early neuronal activity inhibits axon growth. (*a*) Organotypic cocultures of a GFP-expressing EC and a nonfluorescent hippocampus allow for the assessment of single fiber growth speed. See also Fig. S2*a*,*b*. (*b*) Analysis of WT axon growth speed after 3 days in vitro cultivation (DIV3, $n = 41$ axons) and DIV5 ($n = 18$ axons). (c_1) Slower axon growth speed at DIV5 correlated with a shift from a fast advancing category (adv, Mann–Whitney, c_2) to a slow outgrowth category (slow, Mann–Whitney, c_3). See also Fig. S2c. (*d*) Alignment of representative outgrowing fibers over 60 min. Note the decrease in outgrowth speed of DIV5 WT and of DIV3 PRG-$1^{-/-}$ axons. (*e*) Fiber growth speed of DIV3 axons originating from WT and from PRG-$1^{-/-}$ EC slices into a PRG-$1^{-/-}$ hippocampus ($n = 15$ WT axons and 12 PRG-$1^{-/-}$ axons) or into a WT hippocampus ($n = 41$ WT axons and 15 PRG-$1^{-/-}$ axons) assessed in live-imaging experiments. Remarkably, the outgrowth speed of axons originating from PRG-$1^{-/-}$ EC slices was significantly lower independent of the PRG-1 expression in the target region. (f_1) Axon growth speed categories of DIV3 WT and PRG-$1^{-/-}$ axons in % of the live-imaging time. (f_2) The percentage of time PRG-$1^{-/-}$ axons displayed a fast advancing outgrowth was significantly decreased when compared with WT axons. (f_3) In line, the periods PRG-$1^{-/-}$ axons were found in a slow outgrowth category significantly increased. See also Fig. S2d. (g_1) Live imaging of fiber growth before and after application of 500 µM glutamate. Arrows indicate the starting point of growing axons. (g_2) Metric display of fiber growth of the depicted axons over 140 min (70 min control (white); 70 min glutamate application (red)). (*h*) Analysis of fiber growth speed ($n = 14$ WT axons). (*i*) Fiber growth speed at the beginning and the end of glutamate application ($n = 11$ WT axons). All data represent mean ± SEM. For statistical analyses, parametric data were calculated using an unpaired *t*-test or a paired *t*-test when appropriate. *$P < 0.05$; **$P < 0.01$; ***$P < 0.001$.

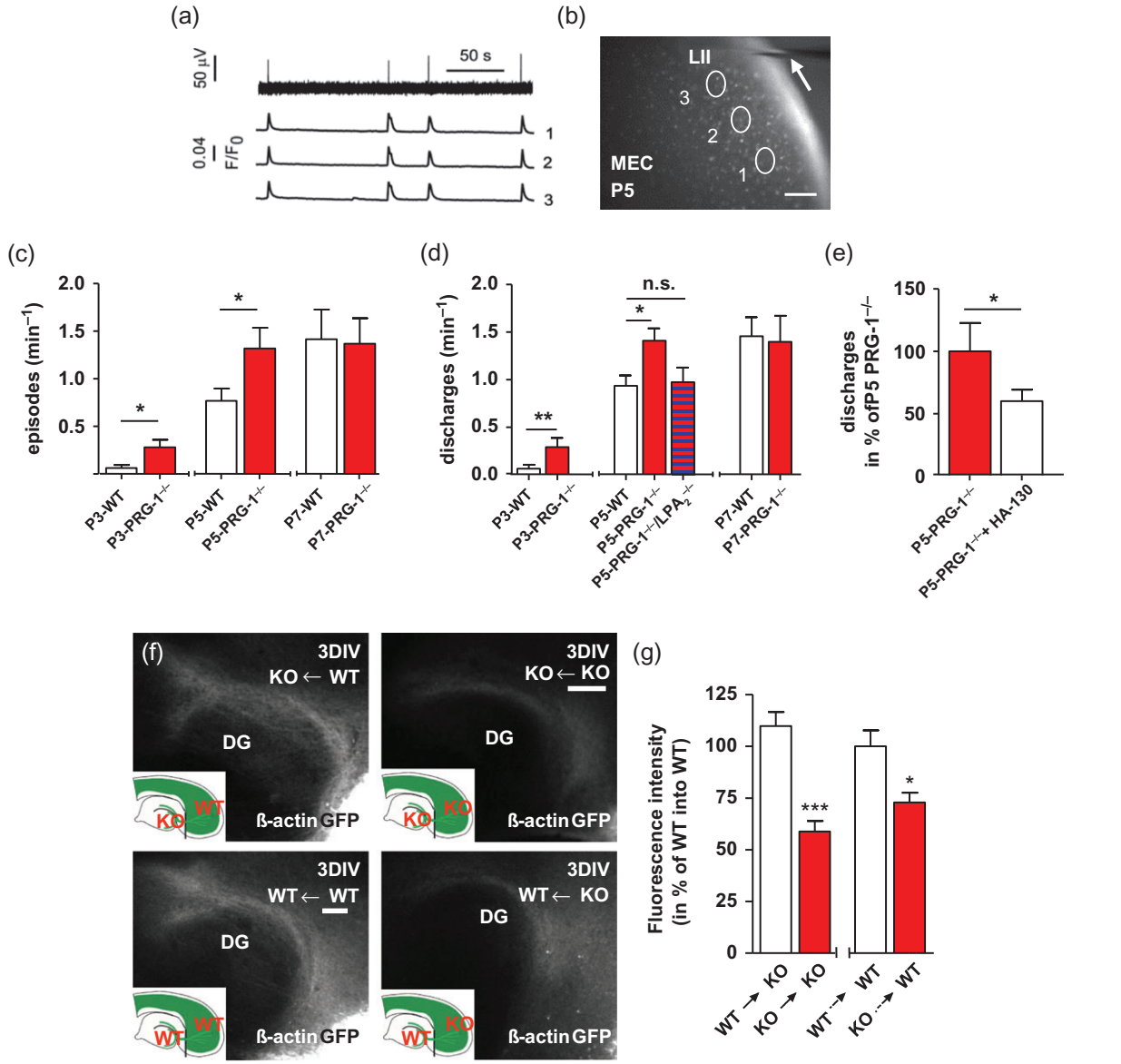

Figure 3. Altered phospholipid signaling prematurely increased excitatory network activity in the MEC decreasing entorhinal projection outgrowth. (*a*) FP discharges (upper trace) and corresponding synchronous Ca^{2+} transients in the depicted ROIs 1–3 shown in *b* correspond to traces 1–3. (*b*) Ca^{2+} imaging in the corresponding ROIs and FP recordings (arrow points to FP pipette) in the MEC. Scale bar: 100 µm. (*c*) FP recordings revealed increased neuronal activity in layer II of the MEC containing PRG-$1^{-/-}$ slices at P3 (P3:12 WT and 16 PRG-$1^{-/-}$ slices, Mann–Whitney test) and at P5 (14 WT and 11 PRG-$1^{-/-}$ slices, *t*-test) but not at P7 (15 WT and 23 PRG-$1^{-/-}$ slices, *t*-test). (*d*) Simultaneous Ca^{2+}-imaging reflected FP recordings showing increased frequency of synchronized discharges in layer II/III of MEC in PRG-$1^{-/-}$ slices at P3 and at P5 but not at P7 (P3, $n = 27$ WT and 30 PRG-$1^{-/-}$ slices, Mann–Whitney test; P5, $n = 33$ WT, 31 PRG-$1^{-/-}$ slices, *t*-test), significance was adjusted for multiple comparisons using Bonferroni correction (P7, $n = 23$ WT and 27 PRG-$1^{-/-}$ slices, Mann–Whitney test). Additional deletion of the LPA_2-R ($n = 42$ slices) normalized discharge frequency in PRG-$1^{-/-}$ slices at P5 to WT levels (Mann–Whitney test). (*e*) Autotaxin inhibition at P5 by 10 µM HA130 significantly decreased the number of synchronous neuronal discharges (Wilcoxon matched-pairs signed rank test; $n = 6$ WT and 6 PRG-$1^{-/-}$ slices). (*f*) Low-magnification brightfield overviews showing GFP-expressing EC slices cultivated with nonfluorescent hippocampal slices. The axonal projection derived from the EC growing towards the DG in the nonfluorescent hippocampus was measured via fluorescence intensity. Entorhinal fiber ingrowth from PRG-$1^{-/-}$ EC slices was significantly lower than the observed fiber ingrowth originating from WT EC slices. To exclude a role of altered attractive properties of targeted granule cell dendrites due to loss of postsynaptic PRG-1, experiments were also done using WT hippocampi (lower row). (*g*) Analysis of fluorescence intensity in percentage of control cocultures (WT EC→WT DG) revealed significantly reduced fiber ingrowth from PRG-$1^{-/-}$ EC cultures independent of PRG-1 expression in the target region ($n = 15$ cultures WT→PRG-$1^{-/-}$; $n = 20$ cultures PRG-$1^{-/-}$→PRG-$1^{-/-}$; $n = 24$ cultures WT→WT; $n = 17$ cultures PRG-$1^{-/-}$→WT; arrows indicate direction of axon growth from EC to DG; *t*-test). Scale bar 100 µm. All data represent mean ± SEM. $^{*}P < 0.05$, $^{**}P < 0.01$,$^{***}P < 0.001$.

speed <50% of the mean speed in the fast advance category was attributed to the slow outgrowth category (category 2). The time when axon growth speed was below 10% of the mean speed in the fast advance category down to 0 µm/h was defined as a pause of axon growth (axon stop category 3). Negative axon growth was regarded as retraction (category 4).

Measurement of Axonal Outgrowth in Collagen-Embedded Slice Cultures

Axon outgrowth assays were performed and analyzed as described (Holtje et al. 2009) using ImageJ. Briefly, EC slices were prepared at postnatal day 0/1 and were embedded in a

collagen I matrix on glass slides and covered with nutrition medium. An inhibitor cocktail containing TTX (1 μM), CNQX (20 μM), and nifedipine (10 μM) (all from Sigma) was added to the cultures that were incubated for 48 h before microscopic analysis. To evaluate the axonal outgrowth of the explants, neurite density was analyzed 100 μm in front of the concave side of the explant with ImageJ. Each data point represents measurements in 1 entorhinal slice culture. Axon outgrowth was normalized to the mean value of the corresponding PRG-1-expressing slices.

Measurement of Axonal Ingrowth of GFP-expressing Axons into the Dentate Gyrus

Experiments were performed according to established protocols (Walsh et al. 2015a; Vogt et al. 2012). Briefly, after 3 days in vitro, (DIV3) or after DIV7, respectively, cultures were fixed with 4% paraformaldehyde (PFA), resliced, coverslipped, and imaged with a fluorescence microscope (Olympus, BX 50) equipped with a Cool SNAP ES digital camera (Roper Scientific). To measure axonal ingrowth, fluorescence intensity of the GFP-positive EC projection was determined in the ML using the software ImageJ or MetaMorph (Molecular Devices). Two regions of interest (ROIs, all ROIs were identical) comprising the full width of the ML were randomly selected in the ML and in the DG. The average fluorescence in the DG was used to determine the background fluorescence, and the difference in fluorescence intensity between the ML and the DG reflected the specific fiber ingrowth in the ML. Data were normalized to the fluorescence intensity of fiber ingrowth of WT→WT (Fig. 3*f*,*g*).

Immunohistochemistry

Cocultures with entorhinal cortices from Thy-1.2-EGFP_L17 mice growing into the PRG-1-deficient hippocampal target tissue (EGFP-negative) were fixed with 4% PFA, resliced, and incubated with an antibody against Calbindin (Swant, Bellinzona) or with accustom-made antibody against PRG-1 (Trimbuch et al. 2009). For developmental expression studies, antibodies against autotaxin (Tanaka et al. 2004), LPA_2-receptor (Trimbuch et al. 2009), VGlut1 (Synaptic Systems), GFAP (DAKO), ß-Gal (Abcam), and Calbindin and Calretinin (Swant) were used. Secondary antibodies Al 488 or AL 568 (Invitrogen) were applied overnight at 4°C. For DAB conversion, biotinylated secondary antibodies were used and DAB-staining was performed as described (Vogt et al. 2012). For assessment of PRG-1 expression, heterozygous PRG-1-deficient mice expressing a ß-Gal reporter were used (for detailed description, see Trimbuch et al., (2009)). Confocal imaging was performed on a Leica TCS SP8 or on a Leica TCS SL confocal laser scanning microscope.

Analysis of Phosphorylation Levels

Western blot analysis of brain lysates or of purified phosphoproteins was performed following standard procedures. Briefly, P5 animals were killed and entorhinal cortices from 2 animals (for WT versus PRG-$1^{-/-}$) or 3 animals (for WT versus LPA_2-$R^{-/-}$ or PRG-$1^{-/-}$/LPA_2-$R^{-/-}$, respectively) were pooled to one biological sample and analyzed as described in the figure legends for the respective experiment. A total of 2.5 mg of protein was then loaded onto the PhosphoProtein purification column (Qiagen). Fractions containing phosphorylated proteins were reduced to 200 μL using Startorius stedim biotech Columns. Protein levels using western blot analysis was performed using following antibodies: CamKI (1:2000; AbCam), Calmodulin (1:1000; Millipore), CamKK (1:500; AbCam), CamKIV (1:1000; Cell Signaling), pCamKI (1:100; provided by Naohito Nozaki and described in Tokumitsu et al., (2004)), LimK1, pLimK1/2, Cofilin and pCofilin (1:1000; Cell Signaling), and beta-actin (1:10.000; MP Biomedicals, LLC). Subsequently, blots were processed for 1 h at room temperature with HRP-conjugated anti-mouse and anti-rabbit secondary antibodies (1:5000; Dianova). Densitometric analyzes were performed using ImageJ.

Viral Infection and Fiber Outgrowth Assessment

Complex hippocampal–entorhinal slice cultures were prepared from E18 pregnant conditional PRG-$1^{fl/fl}$ mice and infected using an AAV expressing mCherry or Cre and mCherry under the synapsin promotor. In the AAVs, a 480 bp fragment of the synapsin (Syn) promoter (Kugler et al. 2003) controlled neuronal expression of Cre-mCherry, whereby a 2A-mediated peptide cleavage linker (Donnelly et al. 2001) was introduced between Cre recombinase and mCherry to enable the production of 2 separate protein products. The production of the $AAV_{1/2}$ EGFP (titer 1.0×10^{11} copies/ml) of the AAV_6 Syn-mCherry (titer 1.05×10^{12} copies/ml) and of the AAV_6 Syn-Cre-mCherry (titer 6.55×10^{11} copies/ml) was performed as previously described (Guggenhuber et al. 2010). After slice preparation, Syn-mCherry, Syn-Cre-mCherry or EGFP expressing AAV were injected at a dilution of 1:5 in the EC using glass pipettes attached to a microinjection device (Toohey Spritzer). In line with recent data (Aschauer et al. 2013), we did not see differences in infection efficiency between these 2 AAV serotypes. After 5 days, in vitro (DIV5) slices were fixed, resliced, and restained for a better visualization of mCherry filled axons (1:1000; Rockland). Fluorescent images were taken on a Leica SP8 equipped with a white light laser and HyD detectors. For visualization of the axonal projection, 7.5 μm thick image stacks were used in the maximal projection. Image analysis was performed with ImageJ. To avoid bias by unspecific background staining, a threshold was measured in areas devoid of axonal projections (e.g., granule cell layer of the DG, which contains the cell bodies) and subtracted from the images. Gray values were measured in the ROIs that comprised the entorhinal performant path projection in the ML of the DG or the infected neurons in the EC. Since AAV application may infect varying amounts of EC neurons, gray values of the EC performant path projection was correlated to the number of infected cells and calculated as a ratio to the gray values of the infected EC-cells. Analysis of PRG-1 expression upon cre-infection was performed by immunofluorescent staining using a custom-made rabbit anti-PRG-1 antibody as described (Trimbuch et al. 2009).

Stereological Analysis of Entorhinal Perforant Path Axons

Myelin staining was performed according to standard procedures and was quantified using unbiased high-precision stereological methods (Vogt et al. 2009). Briefly, brains were cut in serial sections on a vibratome, and every forth section was selected and stained. Definition of the ROI in the hippocampus: EC fibers crossing the hippocampal fissure were stereologically counted. This ROI was delimited by characteristic anatomical formation of the hippocampus and the fimbria. Every second section of the following 10 was used for stereological assessment. The number of EC fibers in individual animals was

normalized to the mean of the WT group or to the mean of the LPA_2-$R^{-/-}$ group representing the strain background.

Statistical Analysis

After assessing for normal distribution (using the Kolmogorov–Smirnov test), statistical analyses between the 2 groups were calculated as using a *t*-test for normal distributed data or with a Mann–Whitney *U* test for nonparametric data. Statistical analyses between more than 2 groups were performed using an one-way analysis of variance with a Bonferroni correction for normal distributed data or a Kruskal–Wallis test and a Dunn's post hoc comparison for nonparametric data. All statistical calculations were performed with GraphPad Software (GraphPad Software, Inc.).

Results

Appearance of Excitatory Activity and Postsynaptic Ca^{2+} Transients in Developing Entorhinal Neurons Depends on Phospholipid Signaling

Periodic spontaneous glutamatergic events in the EC incrementally develop during the first postnatal week (Unichenko et al. 2015) and decrease towards the end of the second postnatal week (Sheroziya et al. 2009). We investigated the role of bioactive phospholipids in regulation of these local excitatory activity and their consequences for circuit formation. To this end, we used PRG-$1^{-/-}$ mice which, at adult ages, were reported to have an increased synaptic lysophospholipid signaling resulting in enhanced presynaptic glutamate release mediated via presynaptic LPA_2-R (Trimbuch et al. 2009).

First, we analyzed neuronal activity at single cell level at P5 in layer II of the EC. PRG-$1^{-/-}$ neurons displayed significant higher mEPSC frequencies with unaltered amplitudes (Fig. 1*a*,*b*, Table S1). Since altered mEPSC frequency implies a presynaptic effect, we measured paired pulse ratios to prove for this assumption. Therefore, we recorded evoked EPSC (eEPCSs) elicited by paired pulse electrical stimulation in the presence of $GABA_A$ receptor blocker gabazine (10 μM, Fig. 1*c*). Paired pulse ratio was significantly higher in wild-type (WT) mice as compared with PRG-$1^{-/-}$ littermates (Fig. 1*c*,*d*). In PRG-$1^{-/-}$, the mean amplitude of eEPSCs was increased, while failure rate, i.e., number of trials in which an electrical pulse failed to elicit the first eEPSC in a pair, was decreased (Fig. 1*e*). These findings reflect an increased basal presynaptic glutamate release and neuronal hyperexcitability of PRG-$1^{-/-}$ developing entorhinal neurons as previously shown for CA1-neurons in adult PRG-$1^{-/-}$ animals (Trimbuch et al. 2009). We next analyzed which type of glutamate receptor mediates the effects of the increased presynaptic release using subtype-specific inhibitors. As the mean amplitude of mEPSCs is small, we recorded eEPSCs at P5, elicited in MEC L2 neurons by electrical stimulation in close proximity to a cell of interest in the presence of gabazine (10 μM), a GABAA receptor blocker. NBQX (10 μM), a selective AMPA (but not kainate) receptor antagonist, completely blocked eEPCSs both in slices from PRG-$1^{-/-}$ animals ($n = 4$), and from their WT littermates ($n = 5$, data not shown). However, NASPM (25 μM), a Ca^{2+}-permeable AMPA receptor blocker failed to affect eEPSCs both in slices from PRG-$1^{-/-}$ animals or from their WT littermates (Fig. S1d,e), suggesting that mostly Ca^{2+}-impermeable AMPA receptors mediate glutamatergic synaptic transmission. UBP302 (10 μM), a selective blocker of kainate receptors, did not influence eEPSC parameters in

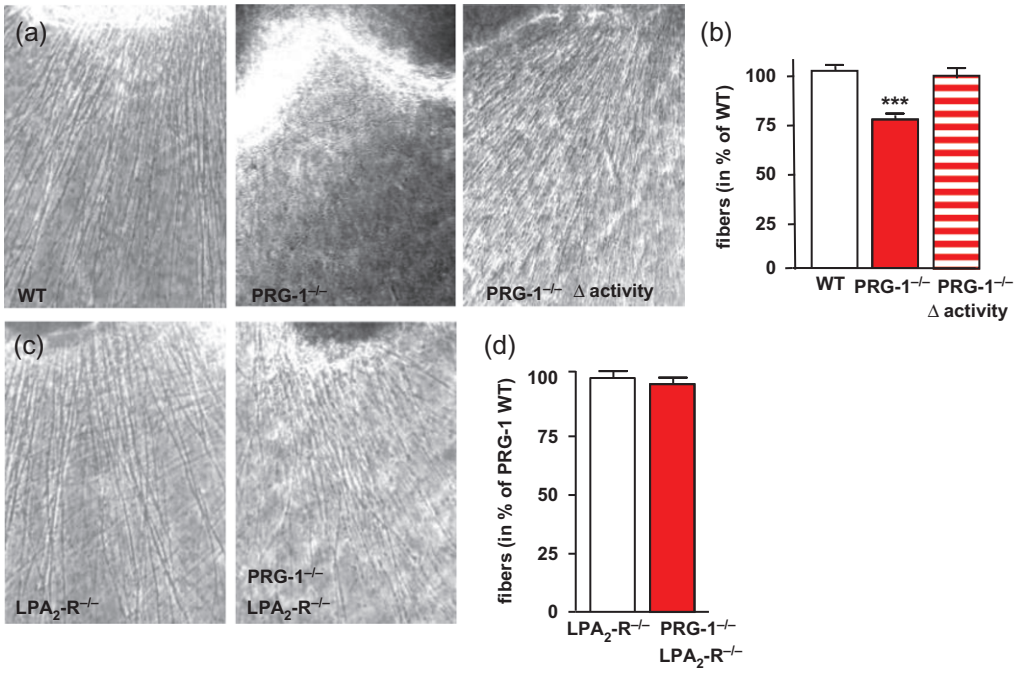

Figure 4. Excitatory neuronal activity mediated via bioactive lipid signaling and involving LPA_2-Rs controls axon outgrowth of the entorhinal projection. (*a*) Axon outgrowth number was lower in PRG-$1^{-/-}$ EC explants (when compared with WT EC explants) and rescued to WT levels upon inhibition of neuronal activity (1 μM TTX, 10 μM Nifedipine, 20 μM CNQX). (*b*) Analysis of axon outgrowth assays revealed complete rescue of PRG-1-deficient explants to WT levels upon electrical activity blockade ($n = 73$ WT, 93 PRG-$1^{-/-}$ and 37 PRG-$1^{-/-\Delta activity}$ explants; one-way analysis of variance with Bonferroni correction). (*c* and *d*) Axon outgrowth number was similar in EC explants from PRG-1-expressing and PRG-1-deficient animals raised on an LPA_2-$R^{-/-}$ background ($n = 106$ LPA_2-$R^{-/-}$ and 95 PRG-$1^{-/-}$/LPA_2-$R^{-/-}$ explants; *t*-test). For better comparison, values in *b* and *d* were normalized to the mean of the PRG-1 expressing explants (to WT or to LPA_2-R explants, respectively). All data represent mean ± SEM. ***$P < 0.001$.

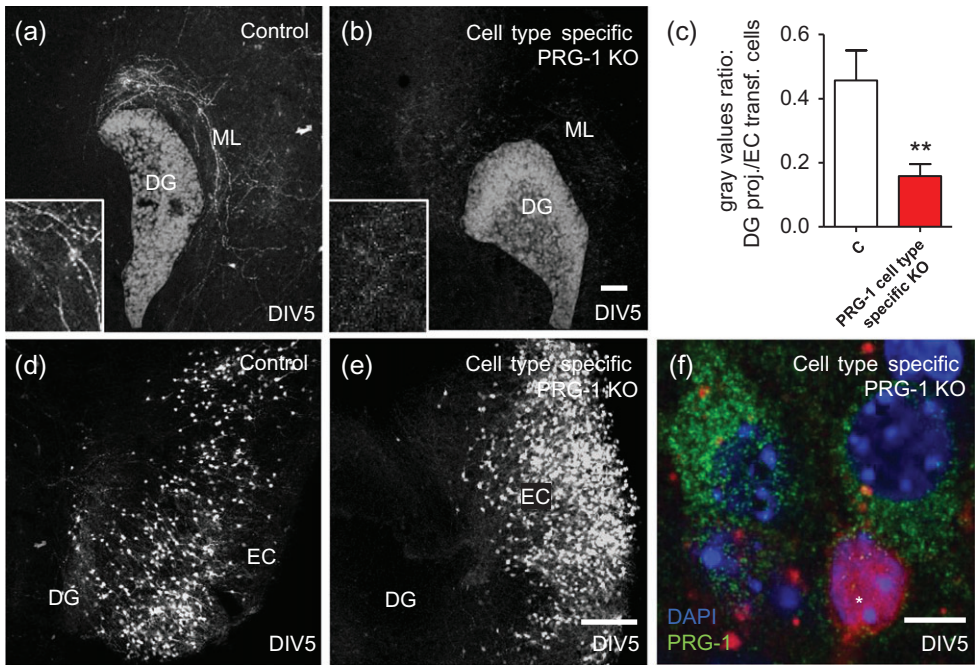

Figure 5. Cell-type-specific PRG-1 deletion decreases axon outgrowth. (*a*) Viral infection of EC neurons using an AAV expressing EGFP resulted in a laminated perforant path projection after 5 days in vitro (DIV5), which was visible in the ML of the DG. DAPI-stained DG was overlayed for better orientation. (*b*) Under same conditions, viral infection of EC neurons using an AAV expressing mCherry and cre under the synapsin promotor resulted in a sparser perforant path projection. (*c*) Gray value quantification of EC fibers in the ML of the DG normalized to the fluorescence of the corresponding infected EC-cells (shown in *d* and *e*) revealed a significant decrease of the perforant path projection after cell-type-specific PRG-1 deletion ($n = 6$ control (*c*) and 8 cell-type-specific PRG-1 KO slices; Mann–Whitney test). (*d* and *e*) Images of infected EC neurons, which are the origin of the neuronal projection depicted above. (*f*) PRG-1 expression was clearly decreased in AAV cre-infected and mCherry-expressing neurons (here, exemplarily shown and marked with a star), while close-by located non-infected neurons displayed strong PRG-1 expression. All data represent mean ± SEM. $^{**}P < 0{,}01$, Scale bar: *a* and *b*: 50 µm; *d* and *e*: 100 µm; *f*: 5 µm.

PRG-$1^{-/-}$ animals or in WT littermates (Fig. S1f,g). As both substances did not affect PPR, the presynaptic expression of functional kainate and/or Ca^{2+}-permeable AMPA receptors appears to be unlikely. From these data, we conclude that contributions of both kainate and Ca^{2+}-permeable AMPA receptors to glutamatergic transmission in L2 of mEC at P5 is minor and that postsynaptic responses are predominantly mediated by Ca^{2+}-impermeable AMPA receptors.

Analyses of active cells in layer II of PRG-$1^{-/-}$ MEC slices using Ca^{2+} imaging revealed significantly increased percentage of active cells exhibiting Ca^{2+} transients at P3 and at P5 reflecting increased discharge rates in the MEC layer II neurons (Fig. 1*f*). This shows that immature entorhinal neuron activity is regulated by bioactive phospholipids. Altered phospholipid signaling results in higher basal glutamate release that augments the neuronal firing probability leading to increased Ca^{2+}-concentrations in individual neurons.

Premature Onset of Excitatory Activity in Entorhinal Neurons Alters Axon Outgrowth

Neuronal activity was shown to affect axon outgrowth in different systems (Gomez and Spitzer 1999; Mire et al. 2012). We therefore established 2-photon live-imaging in organotypic entorhinal–hippocampal cocultures (Fig. 2*a*, S Movie1), which maintain all elements of the trisynaptic hippocampal circuitry and are regarded as an ex vivo model displaying a comparable development of the entorhinal projection to the situation in vivo (Frotscher et al. 2000). Organotypic slice cultures were prepared from newborn mice, when entorhinal axons start to enter the dentate gyrus (Del Rio et al. 1997). Ingrowing axons were imaged after 3 days in vitro (DIV3, which is comparable with P3 in vivo (see also Fig. S2*a*,*b*), when excitatory activity of entorhinal neurons was almost not present, and at DIV5 (comparable with P5 *in vivo*), when robust excitatory discharge activity was observed in WT animals. Axon growth velocity at DIV5 (when entorhinal axons started to contact their targets, the granule cell dendrites (Frotscher et al. 2000)) was significantly decreased when compared with DIV3 (Fig. 2*b*). This decrease of axon growth speed at arrival in its synaptic target region is in line with axon behavior described in other systems (Stamatakou et al. 2015). Thus, decreased axon growth speed at DIV5 correlates with increased Ca^{2+} transients in WT slices at P5 (Fig. 3*d*). In order to understand the mechanisms underlying these developmental changes, we performed detailed analyses of axon growth. Since axon growth is not uniform but rather complex containing periods 1, where axons display a fast outgrowth, 2, where axon growth speed slows down or 3, where axons stop growing or 4, even retract, we have analyzed axon outgrowth according to these categories. Detailed analysis of axon outgrowth dynamics revealed that increased discharge activity of entorhinal neurons at DIV5 (when compared with DIV3) significantly altered pattern switching axon growth from a fast advancing category (adv) to a slow outgrowth category (slow) (Fig. $2c_{1–3}$), Here, axon growth speed was more than 50% slower than in the fast advancing category (Fig. S2c). Interestingly, DIV5 axons displayed a significant decrease in axon outgrowth speed in the fast advancing category, while the axon growth speed in the slow category was not changed pointing to the fact that increased synchronized neuronal activity specifically affected periods of fast axon outgrowth (Fig. S2c).

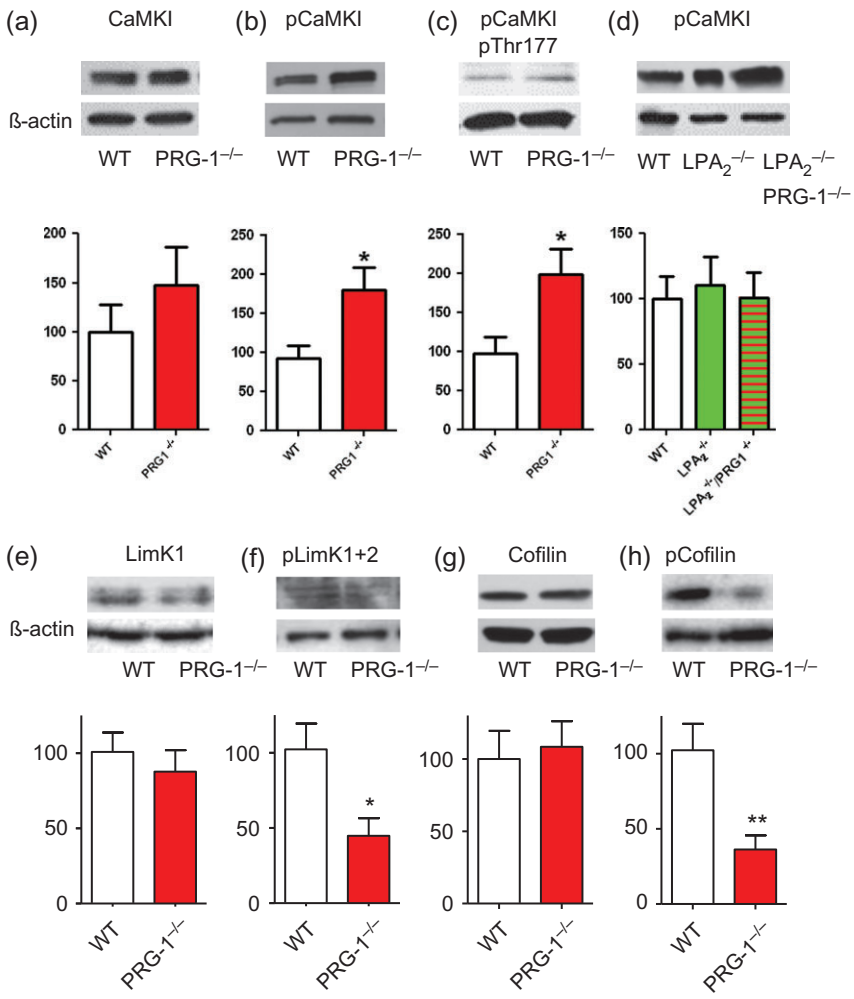

Figure 6. Premature synchronized early neuronal activity affects axon outgrowth related downstream Ca^{2+}-signaling. (*a*) Region specific analysis of the EC at P5 revealed an unaltered total amount of CaMKI ($n = 5$ samples, each sample containing entorhinal cortices from 2 animals). (*b*) Phosphoprotein purification revealed a significant increase of CaMKI in the EC of PRG-$1^{-/-}$ animals ($n = 6$ samples as described above). (*c*) Application of a specific antibody against phosphorylated Thr177 confirmed higher amount of phosphorylated CaMKI in the EC of PRG-$1^{-/-}$ animals ($n = 7$ samples as described above, see also Fig. S3e). (*d*) In line with normalized neuronal activity and rescued axonal outgrowth, PRG-1 deletion on an LPA_2-$R^{-/-}$ background did not influence the amount of phosphorylated CaMKI ($n = 5$ samples, each sample containing entorhinal cortices from 3 animals for each genotype). (*e* and *f*) Analysis of downstream targets directly modulating actin cytoskeleton polymerization revealed normal LimK1 protein levels ($n = 6$ WT and 4 PRG-$1^{-/-}$ samples) but reduced presence of phosphorylated LimK1/2 ($n = 10$ WT and 7 PRG-$1^{-/-}$ samples). (*g* and *h*) in line, total cofilin levels were not altered ($n = 5$ WT and PRG-$1^{-/-}$ samples), while phosphorylated cofilin levels ($n = 7$ WT and PRG-$1^{-/-}$ samples) were decreased. Error bars represent SEM. For comparison of the 2 groups, normal distributed data were analyzed using a *t*-test; nonparametric data were analyzed using a Mann–Whitney test. Comparisons of more than 2 groups (Fig. 6*d*) were performed using a one-way analysis of variance with Bonferroni correction $^*P < 0.05$; $^{**}P < 0.01$. See also Figure S4.

To assess the impact of premature onset of excitatory activity of entorhinal neurons on their axon growth in PRG-$1^{-/-}$ mice, we analyzed axon outgrowth in slices of PRG-$1^{-/-}$ mice at DIV3 and found growth rates that were 25% below the rates of axons derived from WT slices of the same age (Fig. 2*d*,*e*). Interestingly, growth rates of PRG-$1^{-/-}$ axons were significantly lower independent whether the target region, here the hippocampus, was derived from PRG-1 expressing or from PRG-1-deficient mice (Fig. 2*e*). These findings argue against a change in attractive properties of the target region in PRG-$1^{-/-}$ mice as an underlying cause for the observed changes. To exclude possible bias by transient PRG-1 expression in the growth cone, which might account for a decreased outgrowth speed of axons derived from PRG-$1^{-/-}$ neurons, we analyzed WT growth cones in detail but found no PRG-1 expression in these structures (Fig. S2*e*–*h*). Moreover, analysis of growth categories revealed that DIV3 axons derived from PRG-$1^{-/-}$ entorhinal neurons displayed a similar switch from a fast advancing category towards a slow outgrowth category as observed for DIV5 WT-fibers (Fig. 2$f_{1–3}$). This suggests a specific role of increased discharge activity as cause for decreased outgrowth of axons originating from PRG-$1^{-/-}$ entorhinal neurons. In line, outgrowth speed of axons originating from PRG-$1^{-/-}$ neurons was decreased in the fast advancing category, while no changes in outgrowth speed were observed in the slow outgrowth category pointing to a specific effect of neuronal activity and postsynaptic Ca^{2+} increase on fast outgrowing axons (Fig. S2d). Moreover, developmental analysis of the regions where the perforant path originates (the EC) as well as of the region where it terminates and makes synaptic connections [the dentate grus {DG}] did not reveal differences in maturation arguing against bias by an altered maturation of these regions in PRG-$1^{-/-}$ animals (Fig. S2i–l). In sum, our data strongly support the idea that altered synaptic lipid signaling—resulting in an increased

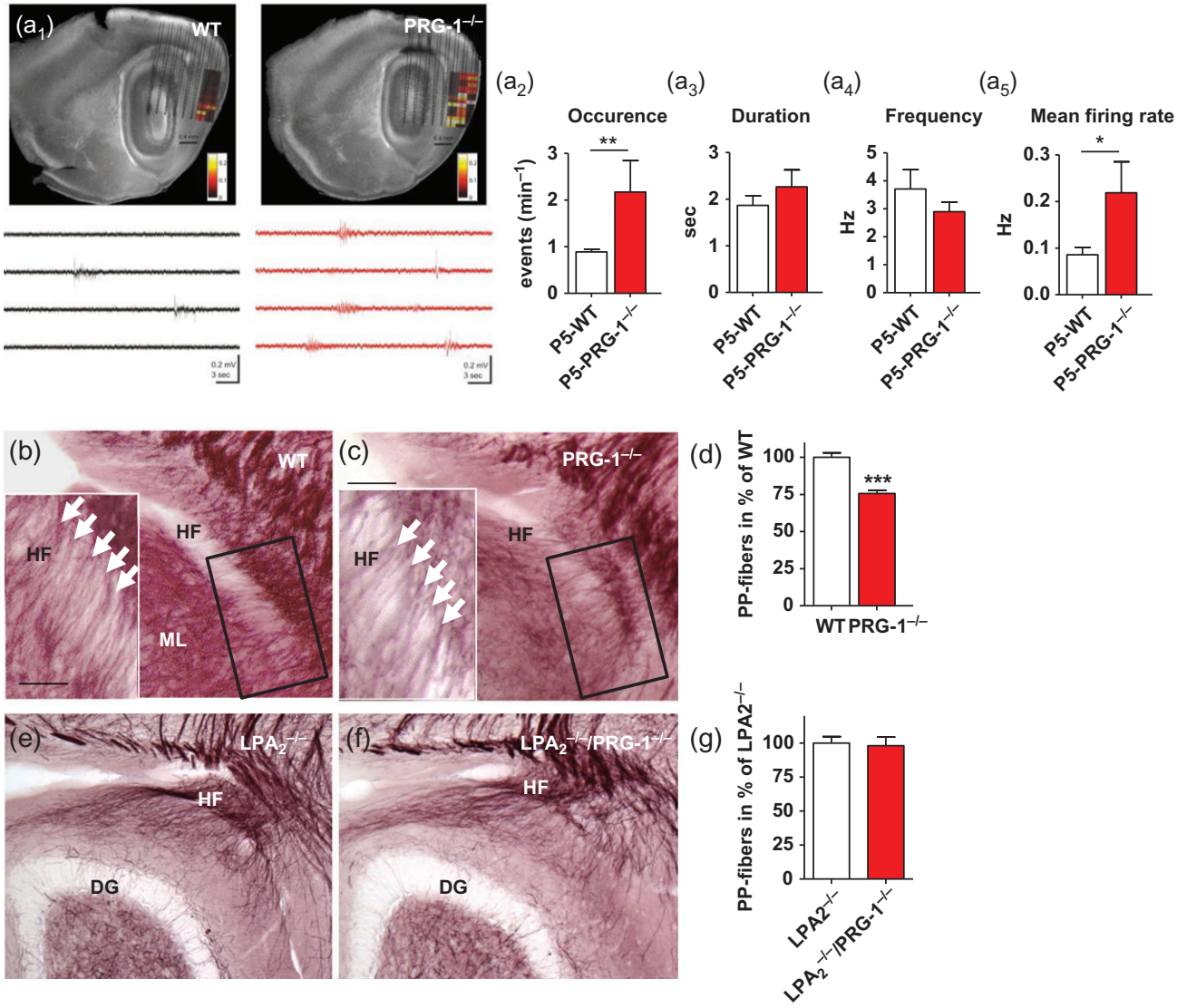

Figure 7. Effects of premature appearance of early neuronal activity in adult mice. (a_1) Digital photomontage showing an 8-shank 128-channel electrode in a DAPI-stained 300 μm thick sagittal section from in vivo recorded P5 WT (left) and PRG-$1^{-/-}$ (right) mice. The right 2 shanks (WT) and the right 3 shanks (PRG-$1^{-/-}$) were located in mEC, and the MUA mean firing rates in each channels are shown in the color plot. Traces below exemplarily show recording from shanks located in the MEC displaying spontaneous activity that was visibly increased in PRG-$1^{-/-}$ mice. (a_{2-4}) Occurrence of spontaneous synchronized neuronal events was significantly higher in PRG-$1^{-/-}$ animals, while duration (a_3) and frequency (a_4) of these MUAs were not altered (n = 8 WT and 7 PRG-$1^{-/-}$ animals). (a_5) MUA mean firing rate in the mEC was significantly higher in PRG-$1^{-/-}$ mice (3) when compared with their WT (4) litters (Data were recorded using a 8 × 16 M probe). (*b* and *c*) Perforant path (PP) projection in WT and PRG-$1^{-/-}$ mice. Inset displays single fibers of the PP (white arrows) in the hippocampal fissure (HF, boxed area). (*d*) Stereological assessment of PP axons in WT and in PRG-$1^{-/-}$ mice (n = 6 WT and 6 PRG-$1^{-/-}$ mice). (*e* and *f*) PP projection in PRG-$1^{+/+}$ and PRG-$1^{-/-}$ mice bred on an LPA_2-$R^{-/-}$ background. (*g*) Stereological assessment of PP axons in WT and in PRG-$1^{-/-}$ mice (n = 6 LPA_2-$R^{-/-}$ and 6 LPA_2-$R^{-/-}$/PRG-$1^{-/-}$animals). Statistical significance was calculated using Student's *t*-test for normally distributed data and Mann–Whitney *U* test for nonparametric data. All data represent mean ± SEM. *P < 0.05; **P < 0.01; ***P < 0.001.

glutamatergic transmission leading to augmented Ca^{2+} levels in the corresponding entorhinal parent neurons—decreased axon outgrowth speed of the entorhinal projection towards the dentate gyrus, its target region.

Since increased discharge activity indicated elevated glutamatergic levels in the MEC of PRG-$1^{-/-}$, we tested this assumption via direct manipulation of axon growth by glutamate application (500 μM). Already 10 min after glutamate application, axon growth rates significantly decreased (Fig. 2g_{1-2}, 2*h*) and remained at low levels throughout the whole experiment (Fig. 2*h*,*i*). Axon growth velocity was not significantly different after 10 and 70 min of glutamate application arguing against a progressive neuronal damage induced by glutamate (Fig. 2*i*).

Premature Onset of Excitatory Activity in Assemblies of Entorhinal Neurons Alters Outgrowth in the Entorhinal–Hippocampal Projection

An increase in mEPSCs leading to neuronal hyperexcitability may affect large group of neurons eventually leading to epileptic discharges (Fang 2016). Therefore, we next analyzed electrical activity of neuronal assemblies in layer II of the medial EC (MEC) and performed field potential (FP) measurements

(Fig. 3*a*). To directly determine affection of postsynaptic Ca^{2+}-levels, we imaged Ca^{2+}-changes in the same MEC slices preparation (Fig. 3*b*). Field potential measurements revealed significantly increased number of events revealing that spontaneous glutamatergic activity affecting large groups of neurons occurs at significantly higher rates in layer II of PRG-$1^{-/-}$ MEC slices at P3 and P5 when compared with the respective WT slices (Fig. 3*c*). These data argue for the fact that synaptic phospholipids that regulate presynaptic basal glutamate release and thereby increase excitatory activity of the single neurons, increase synchronous firing rates of large neuronal populations in the MEC. This supports the general idea that spontaneously active neurons are required for the initiation of synchronous glutamatergic events comprising large groups of neurons. To analyze the effect of bioactive phospholipids on neuronal Ca^{2+} changes following discharges spreading over large areas of the layer II MEC, we analyzed the number of Ca^{2+} transients simultaneously occurring in distant regions of the MEC as depicted in Figure 3*a*,*b*. In line with the results shown in Figure 3*c*, we found highly significant increases in these global events at P3 and at P5 in the MEC of PRG-$1^{-/-}$ mice (for direct comparison of synchronous network discharges at P3, P5, P7, see Fig. S3a). To prove the direct role of synaptic phospholipids and their specific presynaptic LPA_2-R, we further analyzed the occurrence of these global excitatory events in PRG-$1^{-/-}$ animals on an LPA_2-$R^{-/-}$ background (for exemplary presynaptic LPA_2-R expression at P5, see Fig. S3e,f) and found levels that were not different to WT values (Fig. 3*d*, middle) suggesting that premature development of local excitatory networks is mediated via presynaptic LPA_2-Rs. Furthermore, to exclude bias due to an altered amount of presynaptic inputs, we have assessed the dendrite-associated VGlut1-punctae in layer II of the MEC at P5 in WT, PRG-$1^{-/-}$ and LPA$2^{-/-}$ mice finding no difference in presynaptic terminals between these genotypes (Fig. S3g–l). To corroborate the role of LPA_2-R and its cognate ligand LPA, we analyzed phospholipid signal transduction at the level of the LPA-synthesizing enzyme Autotaxin (ATX, for ATX-expression at P5 see Fig. S3d). Therefore, we applied 10 μM HA130, an inhibitor of ATX, able to reduce LPA levels (Albers et al. 2010) and observed a significant decrease of discharge frequency in slices from PRG-$1^{-/-}$ mice at P5 (Fig. 3*e*).

Altogether, we provide mechanistic and molecular evidence at different levels of the LPA/LPA_2-R/PRG-1 axis showing that altered synaptic LPA levels leading to increased basal presynaptic glutamate release eventually induced premature activity of excitatory networks in the EC, which critically affected axon outgrowth.

To prove that not only single axons but also the entire perforant path projection was affected by premature neuronal network activity, we analyzed the development of the whole EC projection using organotypic slice cultures. In this well-established approach (Walsh et al. 2015), axons from EC of β-actin-green fluorescent protein (GFP) expressing animals are growing into hippocampus of β-actin-GFP–negative animals enabling quantitative assessment of ingrowing fibers to their target. In line with the live-imaging data on single axon level (Fig. 2*d*,*e*), the axonal projection derived from PRG-$1^{-/-}$ entorhinal slices was significantly diminished. To prove that this effect indeed resulted from altered lipid signaling, we mimicked this effect in WT slices and treated these organotypic slice cultures with LPA finding a similar effect as observed in PRG-$1^{-/-}$ slices (Fig. S3b,c). Alltogether, these data confirm the inverse relationship of increased excitatory discharge activity in the area of origin, the EC, and the lower outgrowth of the corresponding axonal projection.

Excitatory Activity Mediated by Bioactive Lipid Signaling Controls Axon Outgrowth in the Entorhinal–Hippocampal System

The effect of excitatory discharge activity was further tested on outgrowing axons from EC explants. Quantitative analysis revealed that axon numbers derived from PRG-$1^{-/-}$ EC slices explanted at P1 and cultivated for 48 h (corresponding to P3 in vivo, a time point when discharge activity was almost absent in WT but significantly increased in PRG-$1^{-/-}$ entorhinal slices) was significantly lower but was rescued to WT levels when neuronal activity was blocked by a cocktail containing TTX, CNQX, and nifedipine (Fig. 4*a*,*b*). Since PRG-1-deficiency altered synaptic LPA signaling and application of LPA on WT slices mimicked increased glutamatergic levels present in PRG-$1^{-/-}$ mice (Trimbuch et al. 2009), we investigated whether reduced outgrowth of axons from PRG-$1^{-/-}$ mice was mediated via presynaptic LPA_2-receptors. Using WT and PRG-$1^{-/-}$ mice on an LPA_2-$R^{-/-}$ background that blocks lipid signaling at the presynapse (Trimbuch et al. 2009), we found no more differences between axon outgrowth from WT and from PRG-$1^{-/-}$ slices (Fig. 4*c*,*d*). These results confirm that the PRG-1 effect on axon outgrowth was indeed mediated by presynaptic LPA_2-receptors, which is supported by electrophysiological data showing that LPA_2-receptors mediate premature onset of neuronal activity upon increased lipid signaling in PRG-$1^{-/-}$ mice (Fig. 3*d*).

Cell-type-specific PRG-1 Deletion Reduces EC Axon Outgrowth

We next aimed to provide direct evidence for the role of postsynaptic PRG-1 in axon outgrowth from the EC to the hippocampus. Therefore, we performed cell-type-specific PRG-1 deletion using adeno associated virus (AAV) cre-expression in a subset of entorhinal neurons carrying a floxed PRG-1 gene. The used AAVs (serotype 1/2 or 6) have a similar neuronal infection efficiency in the hippocampus (Aschauer et al. 2013). Cre-expression occurred under the synapsin promotor, thereby limiting cre-expression and PRG-1 deletion to infected neurons. Infected neurons were visualized via enhanced green fluorescent protein (EGFP) or mCherry expression, both well-described fluorescent proteins for axonal studies (Bochorishvili et al. 2014; Liu et al. 2014). These fluorescent proteins were co-expressed by the AAVs and stained cell bodies as well as their axons. Control AAVs expressed EGFP only. As shown in Figure 5*a*, infected EC neurons in control slices (neuronal cell bodies in control slices are shown in Fig. 5d) formed a well-defined axonal projection terminating in the molecular layer (ML) of the DG. However, albeit robust neuronal EC infection by the cre-expressing virus, the perforant path projection originating from the infected and PRG-1-deficient neurons (shown in Fig. 5*e*) was significantly weaker (Fig. 5*b*,*c*). To prove for efficiency of PRG-1 deletion, we resliced and immunostained cre-transfected slices for PRG-1. As shown exemplarily in Figure 5*f*, infected EC neurons identified by mCherry expression were clearly PRG-1 depleted, while unaffected neurons located close to infected cells displayed strong PRG-1 expression. These data argue for a critical role of postsynaptic PRG-1 in controlling synaptic phospholipid signaling, excitatory activity, and Ca^{2+} levels, thereby eventually determining the number of axons that reach their target at a given time during development.

Premature Excitatory Entorhinal Activity Alters Downstream Ca2+-Signaling

Higher presynaptic glutamate release induces higher Ca^{2+}-concentrations in the postsynaptic neuron driving Ca^{2+}-dependent signal transduction (Wayman et al. 2008). However, little is known about the molecular mechanisms induced by higher postsynaptic Ca^{2+}-transients eventually decreasing axon outgrowth. Activity-dependent protein phosphorylation is a key process in regulation and fine-tuning of intracellular functions. We therefore analyzed phosphorylation of downstream molecules of the Calmodulin (CaM)-pathway in the EC of P5 WT and PRG-$1^{-/-}$ animals by phosphoprotein purification and western blotting. Here, we found significantly higher phosphorylation levels of CaMKI, a molecule critically involved in axon outgrowth (Ageta-Ishihara et al. 2009), in PRG-$1^{-/-}$ animals when compared with WT litters (Fig. 6*a*,*b*). In contrast, we found no changes in phosphorylation of other calmodulin kinases (CaM, CamKII, CamKK, CaMKIV, Fig. S4a–d). Higher phosphorylation levels of CaMKI in the EC were further corroborated using a specific antibody against pThr177 (Fig. 6*c*). In addition, using this antibody, we found a similar increase in Thr177 phosphorylation of CaMKI in the phosphoprotein enriched fraction from PRG-$1^{-/-}$ mice and found no signal in the flowthrough-fraction (Fig. S4e). This corroborates the above-mentioned results and points to an effective phosphoprotein purification procedure. Since neuronal hyperexcitation in PRG-$1^{-/-}$ mice required activation of presynaptic LPA_2-R (Trimbuch et al. 2009) and additional deletion of this receptor reduced neuronal activity in PRG-$1^{-/-}$ slices (Fig. 3*d*) and rescued the axon growth deficit in PRG-$1^{-/-}$ explants to WT levels (Fig. 4*c*,*d*), we analyzed CaMKI phosphorylation in EC lysate from PRG-$1^{-/-}$ mice on an LPA_2-R-deficient background. Here, we found normal CaMKI phosphorylation (Fig. 6*d*) supporting the idea that normalized neuronal activity in the EC, as present in PRG-$1^{-/-}$/LPA_2-$R^{-/-}$, rescued axon growth via Ca^{2+}-dependent signal transduction.

Since Ca^{2+}-induced signaling was reported to regulate molecules directly involved in remodeling of the axon's actin cytoskeleton like LimK1 (Saito et al. 2013), we analyzed their expression and found significantly decreased levels of phosphorylated LimK1/2 while total protein levels of LimK1 were not altered (Fig. 6*e*,*f*). LimK1 is critically involved in phosphorylation and thereby deactivation of cofilin, which in its active form stimulates actin depolymerization and disruption of actin filaments (Mizuno 2013). Therefore, we further assessed cofilin and its phosphorylation levels finding unaltered protein levels but significantly decreased levels of phosphorylated cofilin (Fig. 6*g*,*h*). This is in line with lower LimK1/2 phosphorylation levels and lower axon growth rates in axons derived from PRG-$1^{-/-}$ slices.

Consequences of Premature Entorhinal Activity for the Adult Brain

To test whether changes in the onset of excitatory activity in assemblies of entorhinal networks also occur in vivo, we recorded spontaneous field potentials in layer II/III of the MEC in living P5 WT and PRG-$1^{-/-}$ mice. As depicted in Figure 7a_1 by color codes reflecting the multiunit electrical activity (MUA) measured by an 8-shank 128-channel electrode, synchronous excitatory network activity was highly present in the EC of PRG-$1^{-/-}$ mice. Quantitative analysis revealed a significantly higher occurrence of discharges and an increased mean firing rate in the MEC of PRG-$1^{-/-}$ mice, confirming the critical role of synaptic bioactive phospholipids in early excitatory network activity in the EC in vivo (Fig. 7$a_{1–5}$).

Next, we assessed the impact of premature network activity for the mature perforant path at a structural level in vivo and quantified this projection in adult animals. Using a chemical staining approach of single axons, we labeled the EC perforant projection, which crosses the hippocampal fissure where it can be visualized at the single fiber level (Fig. 7*b*, black box indicating the hippocampal fissure, and higher magnification of entorhinal axons in the insert). Axon fiber density in PRG-$1^{-/-}$ animals was visibly lower than in WT animals (Fig. 7*c*). Using unbiased high-precision stereological methods and serial sections, we assessed the number of axons per animal crossing the hippocampal fissure. To compare the results independently of the animal background, we calculated fiber number per animal as a percentage of control fibers and found a significant lower number of axons in PRG-$1^{-/-}$ mice compared with their WT litters (Fig. 7*d*). Since additional LPA_2-R deletion restored early excitatory activity in the EC and axonal outgrowth to WT levels, we analyzed axon fiber numbers in WT and PRG-$1^{-/-}$ mice on an LPA_2-$R^{-/-}$ background (Fig. 7*e*,*f*). We found no longer differences as seen in PRG-$1^{-/-}$ mice (Fig. 7*g*) confirming the effect of premature increase of entorhinal activity on circuit formation up to adult ages.

Discussion

Our study demonstrates that bioactive phospholipids modulate the onset of early neuronal activity in the developing EC and play a critical role in the formation of proper entorhinal–hippocampal connectivity. This was mediated by glutamate-dependent Ca^{2+}-signaling in entorhinal neurons via CaMKI and downstream pathways involving LimKI and cofilin, controlling the stability of the axonal cytoskeleton. Proper appearance of excitatory entorhinal network activity comprising large groups of neurons during critical periods of the development of the entorhinal projection to the hippocampus is under the control of synaptic phospholipid signaling and regulates the amount of fibers of this projection. The general view on early neuronal activity, so far, focused on defects in circuit formation upon its inhibition (Catalano and Shatz 1998; Hanson and Landmesser 2004). Here, we show that premature induction of entorhinal excitatory activity—by only 2 days before its normal appearance—decreased axon growth thereby causing structural alterations in the adult animal.

Phospholipids Modulate Entorhinal Activity Affecting Axon Outgrowth

Spontaneous network activity in the developing brain is a hallmark of young neuronal circuits and is homeostatically regulated (Hanson and Landmesser 2004; Blankenship and Feller 2010). Here, we show that the bioactive phospholipid LPA and its postsynaptic regulatory molecule PRG-1 are key players in this homeostatic control within the entorhinal–hippocampal circuit. While genetic studies suggested that spontaneous neuronal activity was sufficient for embryonic fiber tract development (Molnar et al. 2002), recent studies show that increased glutamatergic levels at the somatodendritic compartment inhibited neurite outgrowth (Yamada et al. 2008; Malyshevskaya et al. 2013). This is in line with our live-imaging analysis of outgrowing fibers showing that enhanced glutamatergic activity slows down axon growth, which could be rescued by blocking neuronal activity. Furthermore, our data do not support a negative effect of

putative higher LPA concentrations in the PRG-1-deficient hippocampus on ingrowing entorhinal axons, which is conceivable from other experimental settings (Campbell and Holt 2003), but argue for the critical importance of the degree of glutamatergic activity.

To prove that the observed reduced axon outgrowth was the direct result of increased excitatory drive of the outgrowing postsynaptic neuron, we performed cell-type-specific PRG-1 deletion in entorhinal neurons that are embedded in an otherwise unaltered environment. Hereby, we could show that altered bioactive synaptic lipid signaling due to lack of postsynaptic PRG-1 and subsequent increased excitatory drive (Trimbuch et al. 2009) in transfected neurons were responsible for the observed reduced axon outgrowth effect.

Premature Onset of Excitatory Activity Reduced Axon Outgrowth Via Ca2+-dependent Signaling

It is generally accepted that increased neuronal activity affects gene expression (Greer and Greenberg 2008). To understand the mechanism coupling increased excitatory activity and decreased axon outgrowth on a molecular level, we investigated Ca^{2+}-dependent signal transduction that is activated upon neuronal activity (Wayman et al. 2008). We found a significant phosphorylation increase of CaMKI, but not of other members of the Ca^{2+}/CaM-pathway, which is a critical molecule for axon outgrowth (Ageta-Ishihara et al. 2009). This is in line with recent data showing that phosphorylation of downstream targets of neuronal activity like Ca^{2+}-signaling molecules has to be homoeostatically regulated to assure proper function. Constitutive activation of the CaMKKα leading to hyperphosphorylation of CaMKI (Kaitsuka et al. 2011) or chronic enhancement of CREB activity (Viosca et al. 2009), a downstream target of the CaM kinase, both led to impairment of spatial memory acquisition.

To further understand the downstream Ca^{2+}-signaling up to molecules directly modeling the axon's actin cytoskeleton, we analyzed EC-specific phosphorylation levels of LimK1 which is a target of the Ca^{2+}/Calmodulin-dependent protein kinases (Takemura et al. 2009; Saito et al. 2013) and inactivates cofilin activity via phosphorylation (Mizuno 2013). Cofilin negatively regulates actin dynamics and destabilizes axons via actin depolymerization (Mizuno 2013; Saito et al. 2013). In fact, we could show that both LimK1/2 and cofilin phosphorylation levels were decreased which results in an increased cofilin activity and a negative effect on axon outgrowth (Mizuno 2013; Saito et al. 2013). However, as reported in other systems (Pandey et al. 2007), it is well feasible that in parallel to a reduction of LimK1/2-mediated cofilin phosphorylation, a direct, Ca^{2+}-dependent cofilin dephosphorylation occurs, which results in alterations of axon outgrowth alike.

Premature Excitatory Activity Affects Entorhinal–Hippocampal Networks in Adult Animals

Since dentate gyrus innervation follows a precise spatiotemporal developmental pattern during the early postnatal period (Frotscher et al. 2000), our data imply alterations of the proper connectivity between EC and hippocampus. Since underlying mechanisms inducing premature neuronal activity in the EC occur in the postnatal period, other dentate gyrus input systems developing at earlier stages such as the septohippocampal projection (Linke and Frotscher 1993) playing an important role for hippocampal function (Hangya et al. 2009; Vandecasteele et al. 2014) are supposed to remain unaffected. In sum, our data suggest that synaptic LPA signaling via presynaptic LPA_2-Rs and under physiological control of the postsynaptic PRG-1 molecule regulates early entorhinal excitatory activity affecting neuronal circuit formation important for memory function in adult animals. Since the early postnatal processes studied here in the mouse brain are equivalent to the development in primates (Amaral et al. 2014) and hippocampus-dependent memory emerges during early childhood concomitant with the maturation of hippocampal circuits (Lavenex and Banta Lavenex 2013), our findings imply an important role of proper onset of entorhinal excitatory activity during human brain development involving bioactive lipid signaling, and call for caution in affecting this process by any external intervention.

Supplementary Material

Supplementary data are available at *Cerebral Cortex* online.

Authors' Contributions

J.V., R.N. designed the experiments and wrote the paper. J.V., S.K., B.L., H.J.L., and R.N. contributed to the experimental design, supervised the experiments and the data analysis or editing. J.A. and J.C. provided antibodies and transgenic animals, respectively. L.S., J.-W.Y., P.U., J.C., U.S., A.Pe.,A.Pr., and B.S.B. were involved in the different experiments.

Notes

We thank Dr. D. O'Neill for language editing and N. Nozaki for providing the pCaMKI antibody. This work was supported by the Deutsche Forschungsgemeinschaft (SFB 1080) to JV, RN, BL and HJL, and the European Research Council (ERC-AG "LiPsyD" to RN). *Conflict of Interest*: None declared.

References

Ageta-Ishihara N, Takemoto-Kimura S, Nonaka M, Adachi-Morishima A, Suzuki K, Kamijo S, Fujii H, Mano T, Blaeser F, Chatila TA, et al. 2009. Control of cortical axon elongation by a GABA-driven Ca2+/calmodulin-dependent protein kinase cascade. J Neurosci. 29:13720–13729.

Albers HM, Dong A, van Meeteren LA, Egan DA, Sunkara M, van Tilburg EW, Schuurman K, van Tellingen O, Morris AJ, Smyth SS, et al. 2010. Boronic acid-based inhibitor of autotaxin reveals rapid turnover of LPA in the circulation. Proc Natl Acad Sci USA. 107:7257–7262.

Amaral DG, Kondo H, Lavenex P. 2014. An analysis of entorhinal cortex projections to the dentate gyrus, hippocampus, and subiculum of the neonatal macaque monkey. J Comp Neurol. 522:1485–1505.

Amaral DG, Witter MP. 1989. The three-dimensional organization of the hippocampal formation: a review of anatomical data. Neuroscience. 31:571–591.

Aschauer DF, Kreuz S, Rumpel S. 2013. Analysis of transduction efficiency, tropism and axonal transport of AAV serotypes 1, 2, 5, 6, 8 and 9 in the mouse brain. PloS one. 8:e76310.

Blankenship AG, Feller MB. 2010. Mechanisms underlying spontaneous patterned activity in developing neural circuits. Nat Rev Neurosci. 11:18–29.

Bochorishvili G, Nguyen T, Coates MB, Viar KE, Stornetta RL, Guyenet PG. 2014. The orexinergic neurons receive synaptic input from C1 cells in rats. J Comp Neurol. 522:3834–3846.

Brauer AU, Savaskan NE, Kuhn H, Prehn S, Ninnemann O, Nitsch R. 2003. A new phospholipid phosphatase, PRG-1, is involved in axon growth and regenerative sprouting. Nat Neurosci. 6:572–578.

Campbell DS, Holt CE. 2003. Apoptotic pathway and MAPKs differentially regulate chemotropic responses of retinal growth cones. Neuron. 37:939–952.

Caroni P. 1997. Overexpression of growth-associated proteins in the neurons of adult transgenic mice. J Neurosci Methods. 71:3–9.

Catalano SM, Shatz CJ. 1998. Activity-dependent cortical target selection by thalamic axons. Science. 281:559–562.

Del Rio JA, Heimrich B, Borrell V, Forster E, Drakew A, Alcantara S, Nakajima K, Miyata T, Ogawa M, Mikoshiba K, et al. 1997. A role for Cajal-Retzius cells and reelin in the development of hippocampal connections. Nature. 385:70–74.

Donnelly ML, Luke G, Mehrotra A, Li X, Hughes LE, Gani D, Ryan MD. 2001. Analysis of the aphthovirus 2A/2B polyprotein "eavage" mechanism indicates not a proteolytic reaction, but a novel translational effect: a putative ribosomal "skip". J Gen Virol. 82:1013–1025.

Fang M, Wei JL, Tang B, Liu J, Chen L, Tang ZH, Luo J, Chen GJ, Wang XF. 2014. Neuroligin-1 knockdown suppresses seizure activity by regulating neuronal hyperexcitability. Mol Neurobiol. 53:270–284.

Frotscher M, Drakew A, Heimrich B. 2000. Role of afferent innervation and neuronal activity in dendritic development and spine maturation of fascia dentata granule cells. Cereb Cortex. 10:946–951.

Gomez TM, Spitzer NC. 1999. In vivo regulation of axon extension and pathfinding by growth-cone calcium transients. Nature. 397:350–355.

Greer PL, Greenberg ME. 2008. From synapse to nucleus: calcium-dependent gene transcription in the control of synapse development and function. Neuron. 59:846–860.

Guggenhuber S, Monory K, Lutz B, Klugmann M. 2010. AAV vector-mediated overexpression of CB1 cannabinoid receptor in pyramidal neurons of the hippocampus protects against seizure-induced excitoxicity. PloS one. 5:e15707.

Hangya B, Borhegyi Z, Szilagyi N, Freund TF, Varga V. 2009. GABAergic neurons of the medial septum lead the hippocampal network during theta activity. J Neurosci. 29: 8094–8102.

Hanson MG, Landmesser LT. 2004. Normal patterns of spontaneous activity are required for correct motor axon guidance and the expression of specific guidance molecules. Neuron. 43:687–701.

Holtje M, Djalali S, Hofmann F, Munster-Wandowski A, Hendrix S, Boato F, Dreger SC, Grosse G, Henneberger C, Grantyn R, et al. 2009. A 29-amino acid fragment of Clostridium botulinum C3 protein enhances neuronal outgrowth, connectivity, and reinnervation. FASEB J. 23:1115–1126.

Kaitsuka T, Li ST, Nakamura K, Takao K, Miyakawa T, Matsushita M. 2011. Forebrain-specific constitutively active CaMKKalpha transgenic mice show deficits in hippocampus-dependent long-term memory. Neurobiol Learn Mem. 96: 238–247.

Kugler S, Kilic E, Bahr M. 2003. Human synapsin 1 gene promoter confers highly neuron-specific long-term transgene expression from an adenoviral vector in the adult rat brain depending on the transduced area. Gene Ther. 10:337–347.

Langston RF, Ainge JA, Couey JJ, Canto CB, Bjerknes TL, Witter MP, Moser EI, Moser MB. 2010. Development of the spatial representation system in the rat. Science. 328:1576–1580.

Lavenex P, Banta Lavenex P. 2013. Building hippocampal circuits to learn and remember: insights into the development of human memory. Behav Brain Res. 254:8–21.

Linke R, Frotscher M. 1993. Development of the rat septohippocampal projection: tracing with DiI and electron microscopy of identified growth cones. J Comp Neurol. 332:69–88.

Liu Y, Keefe K, Tang X, Lin S, Smith GM. 2014. Use of self-complementary adeno-associated virus serotype 2 as a tracer for labeling axons: implications for axon regeneration. PloS one. 9:e87447.

Malyshevskaya O, Shiraishi Y, Kimura F, Yamamoto N. 2013. Role of electrical activity in horizontal axon growth in the developing cortex: a time-lapse study using optogenetic stimulation. PloS one. 8:e82954.

Mire E, Mezzera C, Leyva-Diaz E, Paternain AV, Squarzoni P, Bluy L, Castillo-Paterna M, Lopez MJ, Peregrin S, Tessier-Lavigne M, et al. 2012. Spontaneous activity regulates Robo1 transcription to mediate a switch in thalamocortical axon growth. Nat Neurosci. 15:1134–1143.

Mizuno K. 2013. Signaling mechanisms and functional roles of cofilin phosphorylation and dephosphorylation. Cell Signal. 25:457–469.

Molnar Z, Lopez-Bendito G, Small J, Partridge LD, Blakemore C, Wilson MC. 2002. Normal development of embryonic thalamocortical connectivity in the absence of evoked synaptic activity. J Neurosci. 22:10313–10323.

Moser EI, Kropff E, Moser MB. 2008. Place cells, grid cells, and the brain's spatial representation system. Annu Rev Neurosci. 31:69–89.

Okabe M, Ikawa M, Kominami K, Nakanishi T, Nishimune Y. 1997. "Green mice" as a source of ubiquitous green cells. FEBS Lett. 407:313–319.

Pandey D, Goyal P, Siess W. 2007. Lysophosphatidic acid stimulation of platelets rapidly induces Ca2+-dependent dephosphorylation of cofilin that is independent of dense granule secretion and aggregation. Blood Cells Mol Dis. 38:269–279.

Reyes-Puerta V, Sun JJ, Kim S, Kilb W, Luhmann HJ. 2015. Laminar and columnar structure of sensory-evoked multineuronal spike sequences in adult rat barrel cortex in vivo. Cereb Cortex. 25:2001–2021.

Saito A, Miyajima K, Akatsuka J, Kondo H, Mashiko T, Kiuchi T, Ohashi K, Mizuno K. 2013. CaMKIIbeta-mediated LIM-kinase activation plays a crucial role in BDNF-induced neuritogenesis. Genes Cells. 18:533–543.

Sheroziya MG, von Bohlen Und Halbach O, Unsicker K, Egorov AV. 2009. Spontaneous bursting activity in the developing entorhinal cortex. J Neurosci. 29:12131–12144.

Stamatakou E, Hoyos-Flight M, Salinas PC. 2015. Wnt signalling promotes actin dynamics during axon remodelling through the actin-binding protein Eps8. PloS one. 10:e0134976.

Takemura M, Mishima T, Wang Y, Kasahara J, Fukunaga K, Ohashi K, Mizuno K. 2009. Ca2+/calmodulin-dependent protein kinase IV-mediated LIM kinase activation is critical for calcium signal-induced neurite outgrowth. J Biol Chem. 284: 28554–28562.

Tanaka M, Kishi Y, Takanezawa Y, Kakehi Y, Aoki J, Arai H. 2004. Prostatic acid phosphatase degrades lysophosphatidic acid in seminal plasma. FEBS Lett. 571:197–204.

Tokumitsu H, Hatano N, Inuzuka H, Yokokura S, Nozaki N, Kobayashi R. 2004. Mechanism of the generation of autonomous activity of Ca2+/calmodulin-dependent protein kinase IV. J Biol Chem. 279:40296–40302.

Trimbuch T, Beed P, Vogt J, Schuchmann S, Maier N, Kintscher M, Breustedt J, Schuelke M, Streu N, Kieselmann O, et al.

2009. Synaptic PRG-1 modulates excitatory transmission via lipid phosphate-mediated signaling. Cell. 138:1222–1235.

Unichenko P, Kirischuk S, Yang JW, Baumgart J, Roskoden T, Schneider P, Sommer A, Horta G, Radyushkin K, Nitsch R, et al. 2016. Plasticity-Related Gene 1 Affects Mouse Barrel Cortex Function via Strengthening of Glutamatergic Thalamocortical Transmission. Cereb Cortex. 26:3260–3272.

Unichenko P, Yang JW, Luhmann HJ, Kirischuk S. 2015. Glutamatergic system controls synchronization of spontaneous neuronal activity in the murine neonatal entorhinal cortex. Pflugers Archiv. 467:1565–1575.

Vandecasteele M, Varga V, Berenyi A, Papp E, Bartho P, Venance L, Freund TF, Buzsaki G. 2014. Optogenetic activation of septal cholinergic neurons suppresses sharp wave ripples and enhances theta oscillations in the hippocampus. Proc Natl Acad Sci USA. 111:13535–13540.

Viosca J, Malleret G, Bourtchouladze R, Benito E, Vronskava S, Kandel ER, Barco A. 2009. Chronic enhancement of CREB activity in the hippocampus interferes with the retrieval of spatial information. Learn Mem. 16:198–209.

Vogt J, Glumm R, Schluter L, Schmitz D, Rost BR, Streu N, Rister B, Bharathi BS, Gagiannis D, Hildebrandt H, et al. 2012. Homeostatic regulation of NCAM polysialylation is critical for correct synaptic targeting. Cell Mol Life Sci. 69: 1179–1191.

Vogt J, Paul F, Aktas O, Muller-Wielsch K, Dorr J, Dorr S, Bharathi BS, Glumm R, Schmitz C, Steinbusch H, et al. 2009. Lower motor neuron loss in multiple sclerosis and experimental autoimmune encephalomyelitis. Ann Neurol. 66: 310–322.

Walsh JT, Hendrix S, Boato F, Smirnov I, Zheng J, Lukens JR, Gadani S, Hechler D, Golz G, Rosenberger K, et al. 2015. MHCII-independent CD4+ T cells protect injured CNS neurons via IL-4. J Clin Invest. 125:699–714.

Wayman GA, Lee YS, Tokumitsu H, Silva AJ, Soderling TR. 2008. Calmodulin-kinases: modulators of neuronal development and plasticity. Neuron. 59:914–931.

Yamada RX, Sasaki T, Ichikawa J, Koyama R, Matsuki N, Ikegaya Y. 2008. Long-range axonal calcium sweep induces axon retraction. J Neurosci. 28:4613–4618.

Yang JW, An S, Sun JJ, Reyes-Puerta V, Kindler J, Berger T, Kilb W, Luhmann HJ. 2013. Thalamic network oscillations synchronize ontogenetic columns in the newborn rat barrel cortex. Cereb Cortex. 23:1299–1316.